Squeezed-coherent-state generation via four-wave mixers and detection via homodyne detectors

Bernard Yurke
AT&T Bell Laboratories, Murray Hill, New Jersey 07974
(Received 6 February 1985)

Wideband calculations of the response of a homodyne detector to the outputs of various four-wave-mixer configurations are presented. It is shown that the noise-power spectrum of the homodyne detector output can exhibit regions where the noise is greatly reduced below the shot-noise level even at frequencies far from dc. Hence, in the detection of noise squeezing via homodyne detectors, $1/f$ noise and other low-frequency noise sources may be avoided by observing the homodyne detector's noise power at frequencies far from dc.

I. INTRODUCTION

The proposal by Yuen and Shapiro[1] that squeezed coherent states could be generated via degenerate four-wave mixing has triggered experimental efforts directed toward producing squeezed states in this manner.[2–4] Also considerable theoretical work has been devoted toward understanding how the details of the four-wave-mixing process affect the ability of the four-wave mixer[2,5,6] to generate squeezed states. These investigations have primarily concentrated on the degree to which losses in the medium and pump noise affect the ability of the four-wave-mixing process to generate squeezed coherent light.

Yurke has[7] demonstrated that by placing a four-wave-mixing medium in a cavity the degree of squeezing can be greatly enhanced. The analysis was carried out in the narrow-band approximation, in which only the mode oscillating at the pump frequency was considered. Here this work is extended to a wideband analysis. It is shown that the noise-power spectrum of one component of the amplitude of the light leaving the four-wave mixer can exhibit considerable structure, exhibiting noise reduction over some frequency intervals and noise enhancement over others. This work parallels wideband calculations that have been performed for degenerate parametric amplifiers.[8]

In addition to the analysis of the wideband output of some four-wave mixers, the wideband response of a homodyne detector to this output is presented. Yuen and Shapiro[9,10] have pointed out that homodyne detection measures one of two components of the amplitude of the electromagnetic field arriving at the photodetector. More recently Yuen and Chan have shown that quantum and excess noise from the local oscillator can be eliminated by balanced homodyne detection.[11] The technique has been experimentally demonstrated by Abbas, Chan, and Yee.[12] As a result this technique looks very promising as a means of observing noise squeezing. Mandel[13] and Schumaker[14] have also discussed the detection of squeezed states via homodyne detection. In this paper a wideband calculation of the response of a balanced-homodyne detector is carried out for the case when the photodetectors respond to energy flux rather than photon flux, that is, when the photodetectors are bolometers. Since the noise-power spectrum of one component of the light leaving the four-wave mixer can exhibit noise reduction at frequencies far from dc, $1/f$ noise and other forms of noise likely to appear in the output of the homodyne detector near dc can be avoided by looking at the high-frequency components of the detector's output.

After establishing some notation and defining the component operators of the amplitude and the noise-power spectrum of a component of the amplitude, the analysis of the wideband homodyne detector is presented. The analysis of the four-wave mixers will follow last. This will allow a discussion of the output of a four-wave mixer in terms of the response it produces on a physically realizable detector.

II. THE COMPONENTS OF A FIELD MODE AND SQUEEZED COHERENT STATES

In this section the two components of an electromagnetic field mode are introduced, and their noise-power spectra for squeezed coherent states are derived.

To this end, consider a homodyne detector, which through spatial filtering has been made blind to all but one particular radial field mode of the electromagnetic field propagating along the z axis and let the detector accept this mode over some frequency band B. At the aperture of the detector the electric field operator can thus be written

$$\mathbf{E}(x,y,t)=\boldsymbol{\epsilon}(x,y)\int_B d\omega\,\omega^{1/2}[a(\omega)e^{-i\omega t}+a^{\dagger}(\omega)e^{i\omega t}]\ , \tag{2.1}$$

where $\boldsymbol{\epsilon}(x,y)$ specifies the electric field amplitude and polarization across the detector aperture and the creation and annihilation operators satisfy the commutation relations

$$\begin{aligned}&[a(\omega),a^{\dagger}(\omega')]=\delta(\omega-\omega')\ ,\\ &[a(\omega),a(\omega')]=0\ .\end{aligned} \tag{2.2}$$

The operators $X_1(t,\theta)$ and $X_2(t,\theta)$ of the field amplitude components can be introduced by writing $\mathbf{E}(x,y,t)$ in the form

$$\mathbf{E}=\sqrt{2\omega_0}\boldsymbol{\epsilon}(x,y)[X_1\cos(\omega_0 t+\theta)+X_2\sin(\omega_0 t+\theta)]\ , \tag{2.3}$$

where ω_0 is some preferred frequency, say the homodyne detector's local oscillator frequency. From (2.3) and (2.1) explicit expressions for $X_1(t,\theta)$ and $X_2(t,\theta)$ can be obtained.

In particular

$$X_1(t,\theta)=\int_B d\omega \left[\frac{\omega_0+\omega}{2\omega_0}\right]^{1/2} \times[a(\omega_0+\omega)e^{i\theta}e^{-i\omega t}+\text{H.c.}] ,$$
$$X_2(t,\theta)=\int_B d\omega \left[\frac{\omega_0+\omega}{2\omega_0}\right]^{1/2} \times[-ia(\omega_0+\omega)e^{i\theta}e^{-i\omega t}+\text{H.c.}] . \tag{2.4}$$

By taking the band B to be symmetric about ω_0, $X_1(t,\theta)$ and $X_2(t,\theta)$ can be reexpressed in the following useful form:

$$X_1(t,\theta)=\int_0^{\Delta\omega} d\omega[\chi_1(\omega,\theta)e^{-i\omega t}+\text{H.c.}] ,$$
$$X_2(t,\theta)=\int_0^{\Delta\omega} d\omega[\chi_2(\omega,\theta)e^{-i\omega t}+\text{H.c.}] , \tag{2.5}$$

where

$$\chi_1(\omega,\theta)=\left[\frac{\omega_0+\omega}{2\omega_0}\right]^{1/2} a(\omega_0+\omega)e^{i\theta} + \left[\frac{\omega_0-\omega}{2\omega_0}\right]^{1/2} a^\dagger(\omega_0-\omega)e^{-i\theta} ,$$
$$\chi_2(\omega,\theta)=-i\left[\frac{\omega_0+\omega}{2\omega_0}\right]^{1/2} a(\omega_0+\omega)e^{i\theta} + i\left[\frac{\omega_0-\omega}{2\omega_0}\right]^{1/2} a^\dagger(\omega_0-\omega)e^{-i\theta} , \tag{2.6}$$

and $\Delta\omega=B/2$.

Since $X_2(t,\theta)=X_1(t,\theta-\frac{1}{2}\pi)$ the discussion will now be restricted primarily to X_1. In Sec. III it will be demonstrated that a homodyne detector measures $X_1(t,\theta)$ where θ is determined by the local oscillator phase. Having introduced the component operator $X_1(t,\theta)$, the expectation value of $X_1(t,\theta)$ and $X_1^2(t,\theta)$ will be evaluated for a class of squeezed coherent states which will now be defined.

Let $|0_b\rangle$ denote a vacuum state for the annihilation operators $b(\omega)$:

$$b(\omega)|0_b\rangle=0 \quad \text{for all } \omega , \tag{2.7}$$
$$\langle 0_b|0_b\rangle=1 . \tag{2.8}$$

Squeezed coherent states can be generated from this vacuum state via the mode transformation

$$a(\omega_0+\omega)=G(\omega)b(\omega_0+\omega)+M(\omega)b^\dagger(\omega_0-\omega) . \tag{2.9}$$

Under this transformation $|0_b\rangle$, which is a vacuum state for the $b(\omega)$, is a squeezed coherent state for the $a(\omega)$. Four-wave-mixer configurations which are capable of performing the mode transformation (2.9) on an incoming vacuum state will be presented in a later section of this paper. It is worth noting that $G(\omega)$ and $M(\omega)$ are not independent. Since both $a(\omega)$ and $b(\omega)$ must satisfy commutation relations of the form (2.2), one requires

$$|G(\omega)|^2-|M(\omega)|^2=1 \tag{2.10}$$

and

$$G(\omega)M(-\omega)=G(-\omega)M(\omega) . \tag{2.11}$$

From (2.10) and (2.11) one can readily show

$$|G(\omega)|^2=|G(-\omega)|^2 ,$$
$$|M(\omega)|^2=|M(-\omega)|^2 . \tag{2.12}$$

That is, the norms of G and M must be symmetric functions of ω. Substituting (2.9) into (2.6), $\chi_1(\omega,\theta)$ becomes

$$\chi_1(\omega,\theta)=\left[\left[\frac{\omega_0+\omega}{2\omega_0}\right]^{1/2} G(\omega)e^{i\theta} + \left[\frac{\omega_0-\omega}{2\omega_0}\right]^{1/2} M^*(-\omega)e^{-i\theta}\right] b(\omega_0+\omega) + \left[\left[\frac{\omega_0+\omega}{2\omega_0}\right]^{1/2} M(\omega)e^{i\theta} + \left[\frac{\omega_0-\omega}{2\omega_0}\right]^{1/2} G^*(-\omega)e^{-i\theta}\right] b^\dagger(\omega_0-\omega) . \tag{2.13}$$

Since $\chi_1(\omega,\theta)$ is linear in b and $b^\dagger$, it is immediately evident that the expectation value of $X(t,\theta)$ with respect to $|0_b\rangle$ is zero:

$$\langle 0_b|X(t,\theta)|0_b\rangle=0 . \tag{2.14}$$

In fact, it is clear that each of the frequency components

$$\chi_1(\omega,\theta)e^{-i\omega t}+\chi_1^\dagger(\omega,\theta)e^{i\omega t}$$

of $X_1(t,\theta)$ has zero expectation with respect to the state $|0_b\rangle$.

It is straightforward to show that the mean-square deviation of $X(t,\theta)$ from its zero expectation value is given by

$$\langle 0_b|X_1^2(t,\theta)|0_b\rangle = \int_0^{\Delta\omega} d\omega \left\{ |G(\omega)|^2+|M(\omega)|^2 + 2\left[1-\left[\frac{\omega}{\omega_0}\right]^2\right]^{1/2} \times \text{Re}[G(\omega)M(-\omega)e^{2i\theta}]\right\} , \tag{2.15}$$

where use has been made of Eqs. (2.11) and (2.12). Hence, the noise-power spectrum for $X_1^2(t,\theta)$ is given by

$$S(\omega,\theta)=|G(\omega)|^2+|M(\omega)|^2 +2\left[1-\left[\frac{\omega}{\omega_0}\right]^2\right]^{1/2}\mathrm{Re}[G(\omega)M(-\omega)e^{2i\theta}] . \tag{2.16}$$

It will be shown in Sec. III that $S(\omega)$ can be observed directly by feeding the output of a homodyne detector into a spectrum analyzer. Here some properties of $S(\omega,\theta)$ will be pointed out. If one chooses the identity transformation for (2.8), i.e., $G(\omega)=1$, $M(\omega)=0$, then

$$S(\omega,\theta)=1 .$$

Squeezing is said to occur whenever

$$S(\omega,\theta)<1 . \tag{2.17}$$

Under typical experimental circumstances the homodyne detector output frequency $\omega/2\pi$ will extend to tens of kilohertz, while $\omega_0/2\pi$, for visible light, will be of the order of 5×10^{14} Hz. Hence $(\omega/\omega_0)^2$ appearing in (2.16) is much less than unity and can for practical purposes be neglected. The term $[1-(\omega/\omega_0)^2]^{1/2}$ appearing in (2.16) does, however, set a fundamental upper bound on how small $S(\omega,\theta)$ can be made. One can show

$$S(\omega,\theta)\geq\frac{\omega}{\omega_0} , \tag{2.18}$$

the minimum occurring when

$$|G|^2=\frac{1}{2}\left[1+\frac{\omega_0}{\omega}\right] . \tag{2.19}$$

III. WIDEBAND HOMODYNE DETECTION

In this section it is demonstrated that the noise-power spectrum $P(\omega,\theta)$ given by (2.15) can be measured directly by feeding the output of the homodyne detector into a spectrum analyzer. Yuen and Chan have shown that quantum and excess noise from the homodyne detector's local oscillator can be eliminated by balanced-homodyne detection.[11] The wideband analysis of a balanced-homodyne detector using energy flux detectors is presented here. The case when photoemissive detectors, that is, photon flux detectors, are employed will be carried out in the accompanying paper,[15] but to lowest order in ω/ω_0 the results are the same. A balanced-homodyne detector is depicted in Fig. 1. A 50%-50% beam splitter combines the signal beam and the local oscillator beam. The resulting beams a_1 and a_2 are directed towards photodetector 1 and photodetector 2, respectively. The signal proportional to the difference in the signal generated by photodetector 1 and photodetector 2 (difference mode signal) is then delivered as output. Photodetectors with quantum efficiencies less than unity will be considered, but for simplicity it will be assumed that the photodetectors are matched, that is, their quantum efficiencies are equal. Let $d_1(\omega)$ and $d_2(\omega)$ denote the annihilation operators for light entering, respectively, photodetector 1 and photodetector 2. Introducing the positive and negative frequency components of the electric field at photodetector 1,

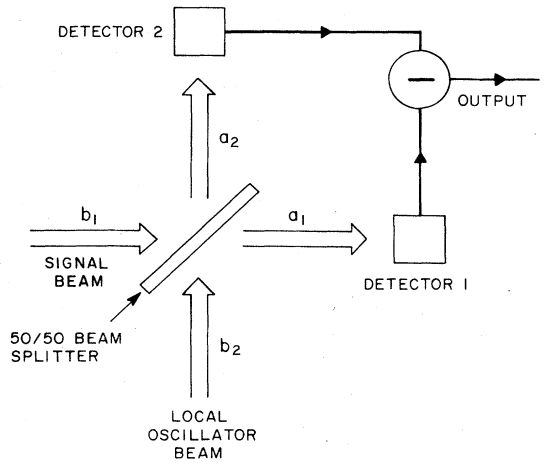

FIG. 1. Balanced-homodyne detector. Output current is proportional to the difference between the photocurrents developed in detectors 1 and 2. Such a detection scheme eliminates noise due to local oscillator intensity fluctuations.

$$\mathbf{E}_1^-=\epsilon(x,y)\int_B d\omega\,\omega^{1/2}d_1^\dagger(\omega)e^{i\omega t} ,$$
$$\mathbf{E}_1^+=\epsilon(x,y)\int_B d\omega\,\omega^{1/2}d_1(\omega)e^{-i\omega t} , \tag{3.1}$$

the power deposited in the bolometric photodetector is proportional to $E_1^-E_1^+$. Let $I_1(t)$ denote the signal delivered by the photodetector to the external world. Then $I_1(t)$ has the form

$$I_1(t)=F\int_B d\omega\int_B d\omega'\omega^{1/2}\omega'^{1/2}d_1^\dagger(\omega)d_1(\omega')e^{i(\omega-\omega')t} , \tag{3.2}$$

where F is the proportionality factor. Similarly, for photodetector 2 one has

$$I_2(t)=F\int_B d\omega\int_B d\omega'\omega^{1/2}\omega'^{1/2}d_2^\dagger(\omega)d_2(\omega')e^{i(\omega-\omega')t} . \tag{3.3}$$

Yuen and Shapiro[9,10] have pointed out that the effect of a quantum efficiency $\eta<1$ for photodetectors can be taken into account by introducing the mode transformations

$$d_1(\omega)=\eta^{1/2}a_1(\omega)+(1-\eta)^{1/2}c_1(\omega) ,$$
$$d_2(\omega)=\eta^{1/2}a_2(\omega)+(1-\eta)^{1/2}c_2(\omega) , \tag{3.4}$$

where $a_1(\omega)$ and $a_2(\omega)$ denote the annihilation operators for light delivered, respectively, to photodetectors 1 and 2. A loss, by the fluctuation-dissipation theorem, couples equilibrium noise into a system. This noise is taken into account with the noise mode operators $c_1(\omega)$ and $c_2(\omega)$ appearing in Eqs. (3.4). For simplicity, η will be taken to be independent of frequency.

Let $b_1(\omega)$ and $b_2(\omega)$ denote the annihilation operators for light propagating along the signal beam and the local oscillator beam, respectively. The mode transformation performed by the 50%-50% beam splitter can be taken to be

$$a_1(\omega)=\frac{1}{\sqrt{2}}[b_1(\omega)+b_2(\omega)]\ ,$$
$$a_2(\omega)=\frac{1}{\sqrt{2}}[-b_1(\omega)+b_2(\omega)]\ . \tag{3.5}$$

Using Eqs. (3.2)—(3.5) one can express the operator $I_1(t)-I_2(t)$, which is proportional to the difference mode signal, in the form

$$\begin{aligned}I_1(\omega)-I_2(\omega)=F\int_B d\omega\int_B d\omega'\omega^{1/2}\omega'^{\,1/2}e^{i(\omega-\omega')t}\\ \times\Bigg[\eta[b_1^\dagger(\omega)b_2(\omega')+b_2^\dagger(\omega)b_1(\omega')]\\ +\left[\frac{\eta(1-\eta)}{2}\right]^{1/2}\Big[b_1^\dagger(\omega)[c_1(\omega')-c_2(\omega')]+b_2^\dagger(\omega)[c_1(\omega')+c_2(\omega')]\\ +[c_1^\dagger(\omega)-c_2^\dagger(\omega)]b_1(\omega')+[c_1^\dagger(\omega)+c_2^\dagger(\omega)]b_2(\omega')\Big]\\ +(1-\eta)[c_1^\dagger(\omega)c_1(\omega')+c_2^\dagger(\omega)c_2(\omega')]\Bigg]\ .\end{aligned} \tag{3.6}$$

Each of the operators $b_1(\omega)$, $b_2(\omega)$, $c_1(\omega)$, and $c_2(\omega)$ acts on a separate Hilbert space. The Hilbert space on which $I_1(\omega)-I_2(\omega)$ acts consists of the outer product of these separate Hilbert spaces.

The expectation of $I_1(\omega)-I_2(\omega)$ is now taken for the state

$$|\psi\rangle=|\psi_1\rangle\,|A_2\rangle\,|0_3\rangle\,|0_4\rangle\ ,$$

where $|0_3\rangle$ and $|0_4\rangle$ are vacuum states for the operators $c_1(\omega)$ and $c_2(\omega)$, respectively, $|\psi_1\rangle$ is an arbitrary state of the Hilbert space of $b_1(\omega)$, and $|A_2\rangle$ acting on $b_2(\omega)$'s Hilbert space represents the state vector for the local oscillator light. For simplicity, let $|A_2\rangle$ be a Glauber state for an oscillator that is very stable and spectrally pure:

$$b_2(\omega)|A_2\rangle=Ae^{-i\theta}\delta(\omega-\omega_0)|A_2\rangle\ . \tag{3.7}$$

One then has

$$\langle\psi|[I_1(\omega)-I_2(\omega)]|\psi\rangle=2^{1/2}\omega_0\eta AF\langle\psi_1|X_1(t,\theta)|\psi_1\rangle\ , \tag{3.8}$$

where

$$X_1(t,\theta)=\int_B d\omega\left[\frac{\omega_0+\omega}{2\omega_0}\right]^{1/2}[b_1(\omega_0+\omega)e^{i\theta}e^{-\omega t}+\text{H.c.}] \tag{3.9}$$

is a component operator for the light in the signal beam, as can be seen by comparison with (2.4). Hence, the balanced homodyne detector measures a component of the incoming signal mode. The precision with which this measurement is carried out is determined by evaluating the higher moments of $I_1(t)-I_2(t)$. In particular, one can show

$$\begin{aligned}\langle\psi|[I_1(t)-I_2(t)]^2|\psi\rangle=2F^2\eta^2A^2\omega_0^2\langle\psi_1|X_1^2(t,\theta)|\psi_1\rangle+F^2\eta(1-\eta)A^2\omega_0\int_B d\omega\,\omega\\ +F^2\eta\int_B d\omega\int_B d\omega'\int_B d\omega''\omega(\omega'\omega'')^{1/2}e^{i(\omega'-\omega'')t}\langle\psi_1|b_1^\dagger(\omega')b_1(\omega'')|\psi_1\rangle\ .\end{aligned} \tag{3.10}$$

From this equation one sees that the rms fluctuations in $X_1(t,\theta)$ are reported by the difference mode signal of the balanced-homodyne detector. The degree to which the rms fluctuations in $I_1(t)-I_2(t)$ reflect the fluctuations in $X_1(t,\theta)$ is degraded by the noise terms in (3.10). By making A sufficiently large, that is, by making the local oscillator beam much more intense than the signal beam, the last term on the right-hand side of (3.10) can be made negligible. The second term on the right-hand side of (3.10),

$$F^2\eta(1-\eta)A^2\omega_0\int_B d\omega\,\omega\ ,$$

arises as a consequence of the less-than-unity quantum efficiency of the homodyne detector and provides a floor below which the noise power of the homodyne detector output cannot be reduced.

Using Eq. (2.15) one can readily show from (3.10) that the noise-power spectrum $S_D(\omega,\theta)$ of $I_1(\omega)-I_2(\omega)$ normalized to unity when the signal beam consists of vacuum fluctuations is

$$S_D(\omega,\theta)=\eta\left\{|G(\omega)|^2+|M(\omega)|^2+2\left[1-\left[\frac{\omega}{\omega_0}\right]^2\right]^{1/2}\times \mathrm{Re}[G(\omega)M(-\omega)e^{2i\theta}]\right\}+1-\eta$$
$$=\eta S(\omega,\theta)+1-\eta\ . \tag{3.11}$$

Hence, it has been demonstrated that the noise-power spectrum (2.16) is directly observable with a homodyne detector. Noise squeezing is observable as a reduction of the $S_D(\omega,\theta)$ below the shot-noise level of unity.

IV. WIDEBAND FOUR-WAVE MIXING

In this section a wideband model for a four-wave-mixing medium is constructed. The treatment follows the approach of Yariv.[16] The medium is taken to be lossless and to have a nonlinear polarization with a third-order polarizability. The pump beam is assumed to be classical. For a treatment of the four-wave-mixing medium from a microscopic point of view the reader is directed to Reid and Walls.[17]

The case when all electric field vectors are polarized along the same direction will be treated. Hence, the nonlinear polarization may be written as

$$P_{\mathrm{nl}}=E^3 d\ . \tag{4.1}$$

By neglecting the effects of losses in the medium, the field equation governing the electric field is

$$\nabla^2 E=\mu\epsilon\frac{\partial^2 E}{\partial t^2}+\mu d\frac{\partial^2 E^3}{\partial t^2}\ . \tag{4.2}$$

The electric field $E(\mathbf{x},t)$ can be separated into the pump field $E_p(\mathbf{x},t)$ and the signal field $E_s(\mathbf{x},t)$,

$$E(\mathbf{x},t)=E_p(\mathbf{x},t)+E_s(\mathbf{x},t)\ . \tag{4.3}$$

The pump electric field, as shown in Fig. 2, arises from two counterpropagating beams at frequency ω_0,

$$E_p(\mathbf{x},t)=\tfrac{1}{2}[E_p(1)e^{i(\mathbf{k}_0\cdot\mathbf{x}-\omega_0 t)}+\mathrm{H.c.}]+\tfrac{1}{2}[E_p(2)e^{-i(\mathbf{k}_0\cdot\mathbf{x}+\omega_0 t)}+\mathrm{H.c.}]\ . \tag{4.4}$$

The pump field will generate a time-dependent susceptibility oscillating at $2\omega_0$. An electric field oscillating at

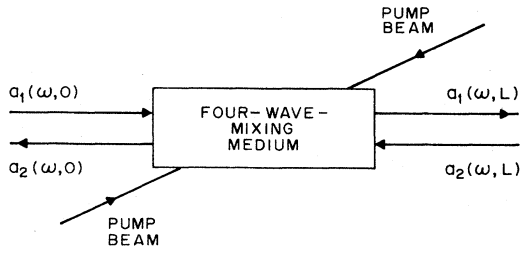

FIG. 2. Four-wave mixer.

$\omega_0+\omega$ will be coupled to a field at $\omega_0-\omega$ and vice versa via the time-dependent susceptibility. Considering the case when all the signal beams propagate along the z axis, in order to study what happens at the frequency $\omega_0+\omega$, E_s must include all the following terms:

$$E_s=\tfrac{1}{2}[E_1(\omega_0+\omega,z)e^{i[k_\omega z-(\omega_0+\omega)t]}+\mathrm{H.c.}]+\tfrac{1}{2}[E_1(\omega_0-\omega,z)e^{i[k_{-\omega}z-(\omega_0-\omega)t]}+\mathrm{H.c.}]+\tfrac{1}{2}[E_2(\omega_0+\omega,z)e^{-i[k_\omega z+(\omega_0+\omega)t]}+\mathrm{H.c.}]+\tfrac{1}{2}[E_2(\omega_0-\omega,z)e^{-i[k_{-\omega}z+(\omega_0-\omega)t]}+\mathrm{H.c.}]\ . \tag{4.5}$$

Where k_ω and $k_{-\omega}$ are taken to be greater than zero and denote the magnitude of the k vectors for light oscillating at $\omega_0+\omega$ and $\omega_0-\omega$, respectively. Making the standard assumption that

$$k_{\pm\omega}\frac{\partial E_s}{\partial z}\gg\frac{\partial^2 E_s}{\partial z^2}\ , \tag{4.6}$$

one obtains, by substituting Eqs. (3.3)–(3.5) into (3.2),

$$\frac{\partial E_1(\omega_0+\omega,z)}{\partial z}=\frac{id}{2}(\omega_0+\omega)\left[\frac{\mu}{\epsilon}\right]^{1/2}E_p(1)E_p(2)\times E_2^\dagger(\omega_0-\omega,z)e^{i(k_{-\omega}-k_\omega)z}\ ,$$
$$\frac{\partial E_2(\omega_0+\omega,z)}{\partial z}=-\frac{id}{2}(\omega_0+\omega)\left[\frac{\mu}{\epsilon}\right]^{1/2}E_p(1)E_p(2)\times E_1^\dagger(\omega_0-\omega,z)e^{-i(k_{-\omega}-k_\omega)z}\ , \tag{4.7}$$

where for simplicity it has been assumed that ϵ is independent of frequency. Introducing the field amplitudes

$$A_l=\left[\frac{n}{\omega_l}\right]^{1/2}E_l \tag{4.8}$$

where n is the index of refraction of the medium, Eqs. (4.7) can be written in the form

$$\frac{dA_1(\omega_0+\omega,z)}{dz}=i\kappa\left[1-\left[\frac{\omega}{\omega_0}\right]^2\right]^{1/2}\times e^{-2i(n/c)\omega z}A_2^\dagger(\omega_0-\omega,z)\ ,$$
$$\frac{dA_2(\omega_0+\omega,z)}{dz}=-i\kappa\left[1-\left[\frac{\omega}{\omega_0}\right]^2\right]^{1/2}\times e^{2i(n/c)\omega z}A_1^\dagger(\omega_0-\omega,z)\ , \tag{4.9}$$

where

$$\kappa=\frac{d}{2}\left[\frac{\omega_0}{\eta_0}\right]^2A_p(1)A_p(2) \tag{4.10}$$

is, in general, a complex number and c is the vacuum speed of light. Equations (4.9) can be integrated as follows.

Let

$$X(z)=A_1(\omega_0+\omega,z)\ ,$$
$$Y(z)=A_2^{\dagger}(\omega_0-\omega,z)\ , \tag{4.11}$$

and

$$a=\kappa\left[1-\left[\frac{\omega}{\omega_0}\right]^2\right]^{1/2}\ ,$$
$$b=\frac{n}{c}\omega\ , \tag{4.12}$$

then Eqs. (4.9) can be reexpressed as

$$\frac{dX(z)}{dz}=iae^{-2ibz}Y(z)\ , \tag{4.13a}$$

$$\frac{dY(z)}{dz}=ia^*e^{2ibz}X(z)\ . \tag{4.13b}$$

These equations readily yield

$$\frac{d^2X}{dz^2}+2ib\frac{dX(z)}{dz}+|a|^2X(z)=0 \tag{4.14}$$

which has the general solution

$$X(z)=Ae^{i[-b+(|a|^2+b^2)^{1/2}]z}+Be^{i[-b-(|a|^2+b^2)^{1/2}]z}\ . \tag{4.15}$$

An expression for $Y(z)$ can be obtained by substituting Eq. (4.15) into Eq. (4.13a).

Taking the nonlinear medium to exist in the region $0<z<L$, the solution to Eqs. (4.9) can be put into the form

$$A_1(\omega_0+\omega,L)=\frac{c(\omega)e^{-ib(\omega)L}A_1(\omega_0+\omega,0)+ia(\omega)e^{-i2b(\omega)L}\sin[c(\omega)L]A_2^{\dagger}(\omega_0-\omega,L)}{c(\omega)\cos[c(\omega)L]-ib(\omega)\sin[c(\omega)L]}\ ,$$
$$A_2^{\dagger}(\omega_0-\omega,0)=\frac{-ia^*(\omega)\sin[c(\omega)L]A_1(\omega_0+\omega,0)+c(\omega)e^{-ib(\omega)L}A_2^{\dagger}(\omega_0-\omega,L)}{c(\omega)\cos[c(\omega)L]-ib(\omega)\sin[c(\omega)L]}\ , \tag{4.16}$$

where

$$a(\omega)=\kappa\left[1-\left[\frac{\omega}{\omega_0}\right]^2\right]^{1/2}\ ,$$
$$b(\omega)=\frac{n\omega}{c}\ , \tag{4.17}$$
$$c(\omega)=[|a(\omega)|^2+b(\omega)^2]^{1/2}\ .$$

In order to use these results as a building block for analyzing cavity four-wave mixers it is convenient to reexpress Eq. (4.16) in terms of creation and annihilation operators that include phase shifts due to position displacements.

Hence the operators

$$a_1(\omega_0+\omega,z)=A_1(\omega_0+\omega,0)e^{ik_\omega z}\ ,$$
$$a_2(\omega_0+\omega,z)=A_2(\omega_0+\omega,0)e^{-ik_\omega z}\ , \tag{4.18}$$

are introduced. Now k_ω is given by

$$k_\omega=\frac{n}{c}(\omega_0+\omega)\ . \tag{4.19}$$

Let θ_0 denote the phase shift experienced by light at frequency ω_0 as it propagates along the length L of the nonlinear medium at frequency ω,

$$\theta_0=\frac{n}{c}\omega_0 L\ . \tag{4.20}$$

Using Eqs. (4.17)–(4.19), Eq. (4.16) can be put into the form

$$a_1(\omega_0+\omega,L)=G_M(\omega)a_1(\omega_0+\omega,0)+M_M(\omega)a_2^{\dagger}(\omega_0-\omega,L)\ ,$$
$$a_2(\omega_0+\omega,0)=M_M(\omega)a_1^{\dagger}(\omega_0-\omega,0)+G_M(\omega)a_2(\omega_0+\omega,L)\ , \tag{4.21}$$

where

$$G_M(\omega)=\frac{c(\omega)e^{i\theta_0}}{c(\omega)\cos[c(\omega)L]-ib(\omega)\sin[c(\omega)L]}\ ,$$
$$M_M(\omega)=\frac{ia(\omega)\sin[c(\omega)L]}{c(\omega)\cos[c(\omega)L]-ib(\omega)\sin[c(\omega)L]}\ . \tag{4.22}$$

Equations (4.21) and (4.22) together with the defining equations (4.17) constitute the major result of this section. The wideband behavior of various four-wave-mixing configurations capable of producing squeezed coherent radiation will now be described.

V. COHERENTLY COMBINING THE OUTPUT BEAMS OF A FOUR-WAVE-MIXING MEDIUM

Yuen and Shapiro[1] have pointed out that squeezed coherent radiation can be generated by coherently combining the output beams of a four-wave-mixing medium via a 50%-50% beam splitter. The device they proposed is depicted in Fig. 3. The input beams $a_1(0)$ and $a_2(L)$ are separated from the output beams $a_2(0)$ and $a_1(L)$ via the optical circulators labeled C. The output beams are then combined via a 50%-50% beam splitter, labeled $M2$. The light in either c_1 or c_2 can exhibit squeezing. A phase shifter ϕ has been included in the figure as a convenient way of simulating what happens when the output beams $a_2(0)$ and $a_1(L)$ travel over different optical path lengths. Letting the beam path labels of Fig. 3 also denote the annihilation operators for the optical modes traveling along the beam path, one has for the phase shifter

$$b_2(\omega_0+\omega)=e^{i\phi(\omega)}a_2(\omega_0+\omega,0)\ . \tag{5.1}$$

Let L_D denote the difference in the length of the optical path followed by light traveling from the four-wave mixer

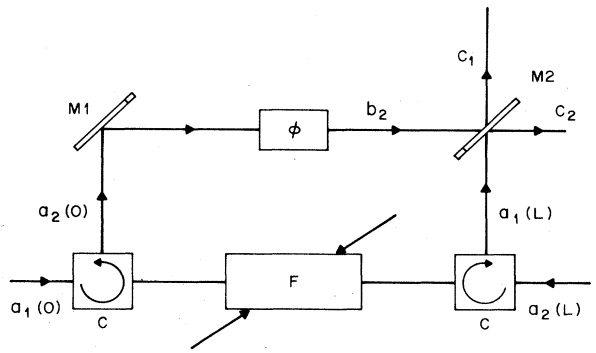

FIG. 3. Four-wave-mixer configuration capable of generating squeezed coherent light. Circulators C are used to separate the light propagating towards and away from the four-wave-mixing medium F. $M2$ is a 50%-50% beam splitter. The phase shifter ϕ simulates the effect of unequal path lengths for the light propagating to $M2$ from the four-wave-mixing medium.

to the 50%-50% beam splitter along beam path $a_2(0)$ and $a_1(L)$. One then has

$$\phi(\omega)=\phi_0+\omega\tau_D \ , \tag{5.2}$$

where

$$\phi_0=\omega_0\frac{L_D}{c} \tag{5.3}$$

is the phase shift at the pump frequency ω_0 and

$$\tau_D=\frac{L_D}{c} \tag{5.4}$$

is the difference in arrival time for pulses propagating along the two optical paths.

For the beam splitter one has

$$c_1(\omega_0+\omega)=\frac{1}{\sqrt{2}}[a_1(\omega_0+\omega,L)+b_2(\omega_0+\omega)] \ ,$$
$$c_2(\omega_0+\omega)=\frac{1}{\sqrt{2}}[-a_1(\omega_0+\omega,L)+b_2(\omega_0+\omega)] \ . \tag{5.5}$$

Equations (5.1) and (5.5) together with Eq. (4.21) can be solved to express the annihilation operators $c_1(\omega_0+\omega)$ and $c_2(\omega_0+\omega)$ in terms of the creation and annihilation operators of the incoming light.

In particular,

$$c_1(\omega_0+\omega)$$
$$=\frac{1}{\sqrt{2}}G_M(\omega)[a_1(\omega_0+\omega,0)+e^{i\phi(\omega)}a_2(\omega_0+\omega,L)]$$
$$+\frac{1}{\sqrt{2}}M_M(\omega)[e^{i\phi(\omega)}a_1^\dagger(\omega_0-\omega,0)+a_2^\dagger(\omega_0-\omega,L)] \ . \tag{5.6}$$

This equation is not of the form (2.9) and hence Eq. (2.16) is not applicable. However, working from the expression given for $X_1(t,\theta)$ in Eq. (2.5), one can show that the noise-power spectrum for the $X_1(t,\theta)$ component of the light in the output beam c_1 is

$$S(\omega,\theta)=|G_M(\omega)|^2+|M_M(\omega)|^2$$
$$+2\left[1-\left[\frac{\omega}{\omega_0}\right]^2\right]^{1/2}\cos(\omega\tau_D)$$
$$\times\mathrm{Re}[e^{i(2\theta+\phi_0)}G_M(\omega)M_M(-\omega)] \ . \tag{5.7}$$

Upon writing $a(\omega)$ in the form

$$a(\omega)=|a(\omega)|e^{i\psi_0} \tag{5.8}$$

and using Eqs. (4.22) the noise-power spectrum can be expressed as

$$S(\omega,\theta)=\frac{c^2(\omega)+|a(\omega)|^2\sin^2[c(\omega)L]}{c^2(\omega)-|a(\omega)|^2\sin^2[c(\omega)L]}-\frac{2[1-(\omega/\omega_0)^2]^{1/2}|a(\omega)|c(\omega)\cos(\omega\tau_D)\sin[c(\omega)L]\sin(2\theta+\phi_0+\theta_0+\psi_0)}{c^2(\omega)-|a(\omega)|^2\sin^2[c(\omega)L]} \ , \tag{5.9}$$

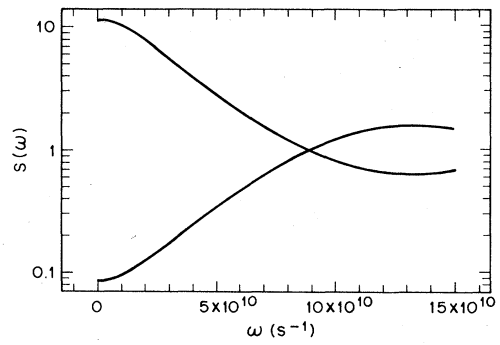

FIG. 4. Noise-power spectrum, for the components of the light leaving port c_1 of the device depicted in Fig. 3, exhibiting the greatest noise squeezing and noise enhancement at $\omega=0$ for the case when the two beam path lengths for light propagating to $M2$ are equal ($L_D=0$) and $L=1$ cm, $n=1$, $\kappa L=1$.

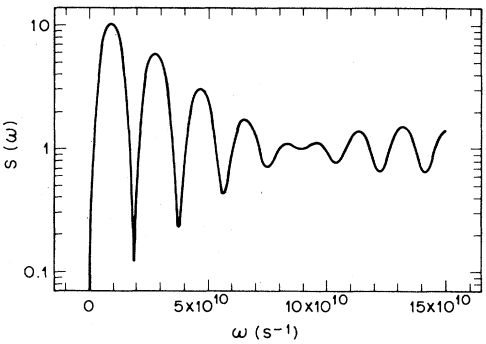

FIG. 5. Noise-power spectrum, for the component of light leaving port c_1, exhibiting the greatest noise squeezing at $\omega=0$, when the two beam path lengths to $M2$ differ by 5 cm ($L_D=10$ cm) and $L=1$ cm, $n=1$, $\kappa L=1$.

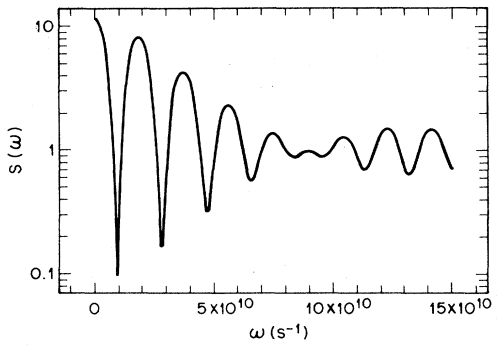

FIG. 6. Noise-power spectrum for the component of light in quadrature (90°) to the component displayed in Fig. 5.

where $a(\omega)$, $b(\omega)$, and $c(\omega)$ are defined by Eqs. (4.17). From Eq. (5.9) one sees that the largest amount of noise squeezing at $\omega=0$ occurs when

$$2\theta+\phi_0+\theta_0+\psi_0=\frac{\pi}{2} . \tag{5.10}$$

This condition may be met by properly adjusting the local oscillator phase θ. Maximum noise enhancement at $\omega=0$ occurs for the component in quadrature to the component exhibiting maximum squeezing, that is,

$$2\theta+\phi_0+\theta_0+\psi_0=-\pi/2 . \tag{5.11}$$

In Fig. 4, Eq. (5.9) is plotted for the components specified by Eqs. (5.10) and (5.11). The length L of the active medium was taken to be 1 cm long. The index of refraction n of the medium was taken to be 1, and the product κL was taken to be 1 and the difference in the beam path lengths L_D was taken to be zero. Note that both components exhibit regions of noise squeezing $S(\omega)<1$ and noise enhancement $S(\omega)>1$. Figures 5 and 6 illustrate the effect of a nonzero path difference L_D. All the parameters for these figures are the same as those for Fig. 4 except now $L_D=10$ cm. Note that the noise-power spectrum of each component exhibits pronounced dips below the shot-noise level $S(\omega)=1$.

When

$$2\theta+\phi_0+\theta_0+\psi_0=0 , \tag{5.12}$$

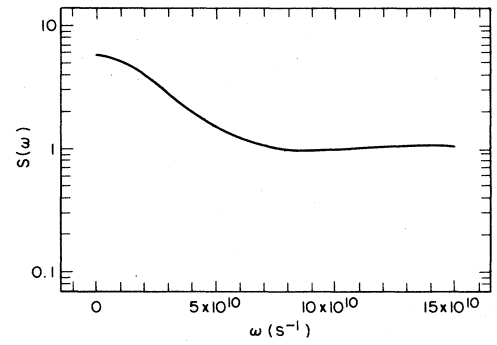

FIG. 7. Noise-power spectrum for the component of light 45° to the component displayed in Fig. 5. No noise squeezing is observed.

the second term of (5.9) vanishes, and, since the denominator of the first term is always less than or equal to the numerator, one has $S(\omega,\theta)\geq 1$ for all ω. In this case $S(\omega,\theta)$ is independent of the path length difference L_D. Figure 7 shows $S(\omega,\theta)$ when (5.12) holds. This figure is plotted for the same parameters used in Figs. 5 and 6.

VI. A FOUR-WAVE-MIXING MEDIUM BACKED BY A TOTALLY REFLECTING MIRROR

In this section a four-wave-mixing medium backed by a totally reflecting mirror is discussed. The device is depicted in Fig. 8. The four-wave-mixing medium acts like a phase-conjugating mirror. This phase-conjugating mirror together with the totally reflecting mirror forms a cavity. As the reflectivity of the phase-conjugating mirror approaches unity the cavity is brought near the threshold of oscillation. In a narrow-band analysis Yurke[7] has shown that a large amount of squeezing is generated in the output beam as threshold is approached. Here the wideband behavior of the device is presented. It is shown that the noise-power spectrum for a component of the output can exhibit rich structure, exhibiting regions of both noise squeezing and noise enhancement.

Let $\theta_1(\omega)$ denote the phase shift suffered by light at frequency $\omega_0+\omega$ as it propagates from the four-wave-mixing medium to the totally reflecting mirror. Then $a_2(\omega_0+\omega, L)$ can be expressed in terms of $a_1(\omega_0+\omega, L)$,

$$a_2(\omega_0+\omega, L)=e^{2i\theta_1(\omega)}a_1(\omega_0+\omega, L) . \tag{6.1}$$

Let L_1 denote the distance between the four-wave-mixing medium and the totally reflecting mirror, then

$$\theta_1(\omega)=\theta_1(0)+\tau_1\omega , \tag{6.2}$$

where

$$\theta_1(0)=\frac{\omega_0 L_1}{c} \tag{6.3}$$

is the phase shift for light at ω_0 and

$$\tau_1=\frac{L_1}{c} \tag{6.4}$$

is the time it takes light to travel from the four-wave-mixing medium to the totally reflecting mirror. Equation (6.2) together with Eq. (4.21) may be solved to yield the outgoing annihilation operators $a_2(\omega,0)$ in terms of the incoming creation and annihilation operators $a_1^\dagger(\omega,0)$ and

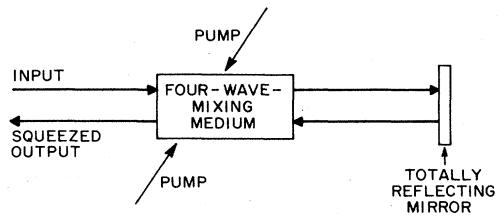

FIG. 8. Four-wave-mixing medium backed with a totally reflecting mirror. Output light exhibits large amounts of squeezing when the reflectivity of the four-wave-mixing medium approaches unity.

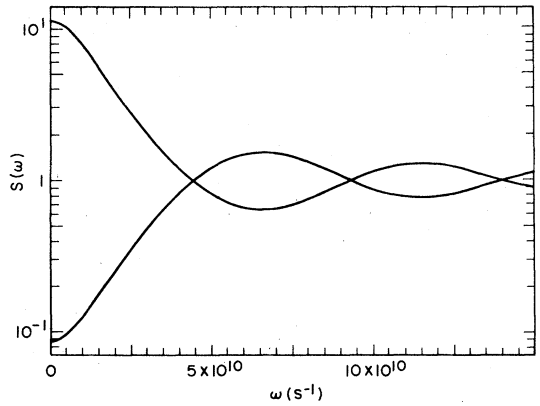

FIG. 9. Noise-power spectrum, for the components of the light leaving the device of Fig. 8, exhibiting the greatest noise squeezing and enhancement at $\omega=0$ for the case when the distance L_1 between the four-wave-mixing medium and the totally reflecting mirror is zero and $L=1$ cm, $n=1$, $\kappa L=0.5$.

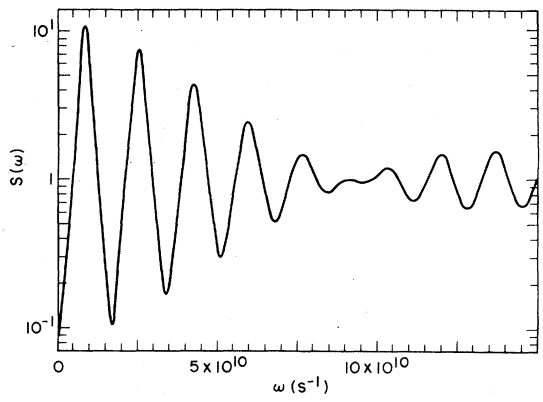

FIG. 10. Noise-power spectrum, for the component of light leaving the device of Fig. 8, exhibiting the greatest noise squeezing at $\omega=0$ for the case when the distance L_1 between the four-wave-mixing medium and the totally reflecting mirror is 5 cm, the other parameters being the same as for Fig. 9.

$a_1(\omega,0)$. The result is

$$a_2(\omega_0+\omega,0)=G_R(\omega)a_1(\omega_0+\omega,0)+M_R(\omega)a_1^\dagger(\omega_0-\omega,0)\ , \tag{6.5}$$

where the amplitude gain $G_R(\omega)$ and reflection amplitude $M_R(\omega)$ for the four-wave mixer with a totally reflecting mirror in terms of the medium's amplitude gain $G_M(\omega)$ and reflection amplitude $M_M(\omega)$ is

$$G_R(\omega)=\frac{e^{i2\theta_1(\omega)}G_M^2(\omega)}{1-M(\omega)M^*(-\omega)e^{i2[\theta_1(\omega)-\theta_1(-\omega)]}}\ ,$$

$$M_R(\omega)=\frac{M_M(\omega)\{1+[G_M(\omega)G_M^*(-\omega)-M_M(\omega)M_M^*(-\omega)]e^{i2[\theta_1(\omega)-\theta_1(-\omega)]}\}}{1-M(\omega)M^*(-\omega)e^{i2[\theta_1(\omega)-\theta_1(-\omega)]}}\ . \tag{6.6}$$

Equation (6.5) is of the form (2.9). Hence, the four-wave mixer backed by a totally reflecting mirror can transform incoming vacuum fluctuations into squeezed states whose noise-power spectrum for a particular component is given by (2.16).

Figure 9 shows the noise-power spectrum $S(\omega)$ for both the component exhibiting maximum squeezing at $\omega=0$ and its quadrature component which exhibits maximum noise enhancement at $\omega=0$. For this simulation, the distance between the mirror and the active medium was taken to be zero. The length L taken to be 1 cm was chosen for the medium, the index of refraction n was set to 1, and the product of κL was taken to be 0.5. More than an order of magnitude in noise reduction is obtained at $\omega=0$. Note that both components exhibit regions of noise squeezing and noise enhancement. Figures 10 and 11 show the effect of moving the totally reflecting mirror away from the four-wave-mixing medium. The distance from the active medium to the totally reflecting mirror was taken to be 5 cm in this case. All other parameters are the same as in Fig. 9. Figure 10 displays the component exhibiting maximum squeezing at the origin. Note the oscillation from maximum squeezing to maximum noise enhancement as a function of ω.

Figure 11 depicts what happens to the component in which the local oscillator phase has been shifted by $\pi/4$ radians from the phase exhibiting maximum squeezing. In this case no noise squeezing is observed. By comparing $S(\omega)$ of Fig. 7 and Fig. 11 one sees that Fig. 11 shows more structure than the corresponding noise-power spectrum for the device discussed in Sec. V.

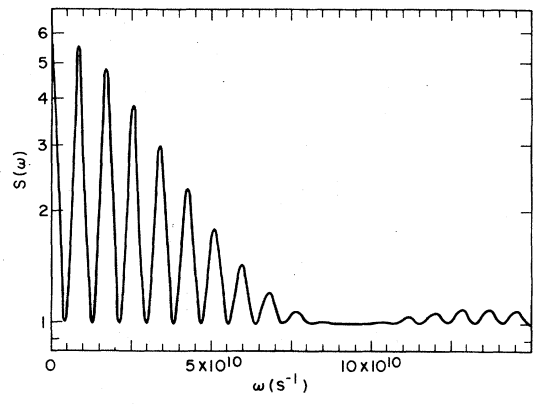

FIG. 11. Noise-power spectrum for the component of light 45° to that depicted in Fig. 10.

VII. THE CAVITY FOUR-WAVE MIXER

In this section a partly transparent mirror is added to the input-output port of the four-wave mixer discussed in Sec. VI. The device is depicted in Fig. 12. Such a configuration allows one to obtain large amounts of squeezing[7] even when the κL product for the four-wave-mixing medium is much less than unity.

The relation between the creation and annihilation operators for light propagating along beam paths a_1 and a_2 have been derived in Sec. VI and are given by Eqs. (6.5) and (6.6).

The distance L_2 between the partly transparent mirror $M1$ and the four-wave mixer is taken into account with the phase shifter θ_2 depicted in Fig. 12. The relation between the a_1,a_2 modes and the b_1,b_2 modes is given by

$$a_1(\omega_0+\omega)=e^{i\theta_2(\omega)}b_1(\omega_0+\omega)\ ,$$
$$b_2(\omega_0+\omega)=e^{i\theta_2(\omega)}a_2(\omega_0+\omega)\ , \tag{7.1}$$

where $\theta_2(\omega)$ in analogy with (6.2) has the form

$$\theta_2(\omega)=\theta_2(0)+\tau_2\omega\ , \tag{7.2}$$

where

$$\theta_2(0)=\omega_0\tau_2\ ,$$
$$\tau_2=\frac{L_2}{c}\ . \tag{7.3}$$

The scattering matrix for the partly transparent mirror

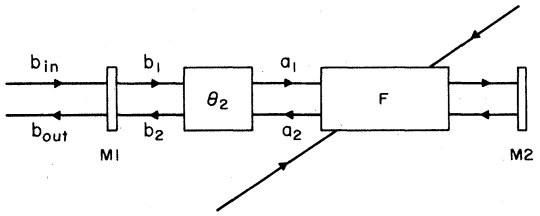

FIG. 12. Cavity four-wave mixer. When κL for the four-wave-mixing medium is small, a large amount of squeezing can still be achieved by passing the light through the medium many times.

$M1$ is taken to be given by

$$b_1(\omega_0+\omega)=K^{1/2}b_{\rm in}(\omega_0+\omega)+(1-K)^{1/2}b_2(\omega_0+\omega)\ ,$$
$$b_{\rm out}(\omega_0+\omega)=-(1-K)^{1/2}b_{\rm in}(\omega_0+\omega)+K^{1/2}b_2(\omega_0+\omega)\ . \tag{7.4}$$

Equations (6.5), (7.1), and (7.4) can be solved to express $b_{\rm out}(\omega)$ in terms of $b_{\rm in}(\omega)$. The result is

$$b_{\rm out}(\omega_0+\omega)=G(\omega)b_{\rm in}(\omega_0+\omega)+M(\omega)b_{\rm in}^{\dagger}(\omega_0-\omega)\ , \tag{7.5}$$

where $G(\omega)$ and $M(\omega)$ have the form

$$G(\omega)=A(\omega)/D(\omega)\ ,$$
$$M(\omega)=B(\omega)/D(\omega)\ . \tag{7.6}$$

The complex numbers $A(\omega)$, $B(\omega)$, and $D(\omega)$ are given by

$$A(\omega)=-(1-K)^{1/2}+G_R(\omega)e^{i2\theta_2(\omega)}+(1-K)G_R^*(-\omega)e^{-i2\theta_2(-\omega)}$$
$$-(1-K)^{1/2}[G_R(\omega)G_R^*(-\omega)-M_R(\omega)M_R^*(-\omega)]e^{i2[\theta_2(\omega)-\theta_2(-\omega)]}\ , \tag{7.7}$$

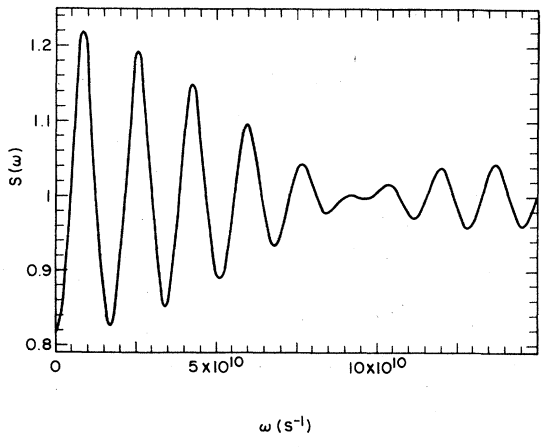

FIG. 13. Noise-power spectrum, for the component of light leaving the device of Fig. 8, exhibiting the greatest noise squeezing at $\omega=0$ for the case when $\kappa L=0.01$, $L=1$ cm, $n=1$, and $L_2=5$ cm.

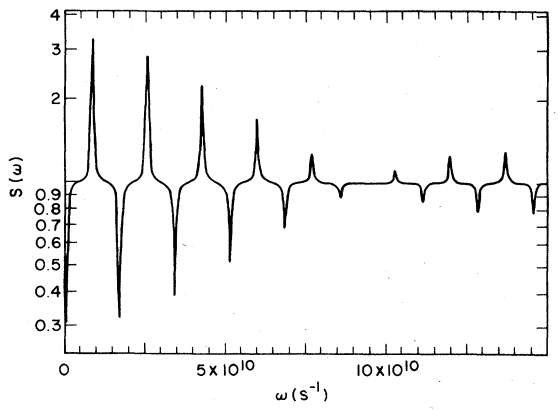

FIG. 14. Noise-power spectrum, for the component of light leaving the device of Fig. 12, exhibiting the greatest noise squeezing at $\omega=0$ when the transmission coefficient K of the mirror $M1$ is 0.5 and the mirror is located a distance L_2 of 5 cm from the four-wave-mixing medium. All other parameters are the same as in Fig. 13. Comparing with Fig. 13, one sees that a substantial enhancement in the amount of squeezing results by putting the mirror $M2$ in place.

$$B(\omega)=KM_R(\omega)e^{i[\theta_2(\omega)-\theta_2(-\omega)]}, \tag{7.8}$$

$$D(\omega)=1-(1-K)^{1/2}[G_R(\omega)e^{i2\theta_2(\omega)}+G_R^*(-\omega)e^{-i2\theta_2(-\omega)}] +(1-K)[G_R(\omega)G_R^*(-\omega)-M_R(\omega)M_R^*(-\omega)]e^{i2[\theta_2(\omega)-\theta_2(-\omega)]}. \tag{7.9}$$

As an illustration of the enhancement in noise squeezing that can be achieved, consider the device discussed in Sec. VI, where $L=1$ cm, $n=1$, $L_1=5$ cm, and the κL product is now taken to be 0.01, a factor of 50 less than that chosen to generate Fig. 10. The output of this device is depicted in Fig. 13. The noise level at $\omega=0$ drops only to 0.82, unity being the vacuum fluctuation level.

By placing a mirror with a transmission coefficient $K=0.5$ at a distance $L_2=5$ cm in front of the four-wave mixer, the noise level at $\omega=0$ drops to the respectable value of 0.32, as depicted in Fig. 14. One also has a corresponding enhancement of the noise peaks and dips away from $\omega=0$. These peaks and dips are spaced with a frequency spacing $\Delta\omega$ corresponding to the difference in frequency between two successive Fabry-Perot modes.

VIII. CONCLUSION

A wideband model for a balanced homodyne detector has been presented. It was shown that the homodyne detector measures a component $X_1(t,\theta)$ of the incoming signal light. An expression for the noise-power spectrum of the output of a homodyne detector has been obtained for the case when the incoming light consists of squeezed vacuum fluctuations. Expressions for the wideband output of various four-wave-mixer configurations capable of squeezing light have been presented. It has been shown that the noise-power spectrum of the $X_1(t,\theta)$ component of the squeezed output light can show considerable structure as a function of frequency. In particular $S(\omega,\theta)$ for a given θ generally shows regions of noise squeezing $S<1$ and regions of noise enhancement $S>1$. These features may facilitate the experimental observation of squeezed coherent light since $1/f$ noise and other forms of low-frequency noise originating in the homodyne detector can be avoided by observing $S(\omega,\theta)$ at frequencies sufficiently far from dc. For the convenience of display, cavity path lengths comparable to the 1-cm path length of the four-wave-mixing medium were chosen to generate the figures. For cavities of such dimensions, $S(\omega)$ exhibits successive dips on the GHz frequency scale, frequencies above the response range of present photodetectors. Experimentally it is more convenient to work with cavities a meter long or longer. For such cavities $S(\omega)$ will show successive dips and peaks on the 10—100-MHz frequency scale, a range easily accessible with the current generation of photodetectors.

[1]H. P. Yuen and J. H. Shapiro, Opt. Lett. **4**, 334 (1979).
[2]R. S. Bondurant, Ph.D. thesis, Massachusetts Institute of Technology, 1983.
[3]R. E. Slusher, B. Yurke, and S. F. Valley, J. Opt. Soc. Am. B **1**, 525 (1984).
[4]M. D. Levenson, J. Opt. Soc. Am. B **1**, 525 (1984).
[5]G. J. Milburn, D. F. Walls, and M. D. Levenson, J. Opt. Soc. Am. B **1**, 390 (1984).
[6]P. Kumar and J. H. Shapiro, Phys. Rev. A **30**, 1568 (1984).
[7]B. Yurke, Phys. Rev. A **29**, 408 (1984).
[8]M. J. Collett and C. W. Gardiner, Phys. Rev. A **30**, 1386 (1984); C. W. Gardiner and C. M. Savage, Opt. Commun. **50**, 173 (1984).
[9]H. P. Yuen and J. H. Shapiro, IEEE Trans. Inf. Theory **IT-26**, 78 (1980).
[10]J. H. Shapiro, H. P. Yuen, and J. A. Machado Mata, IEEE Trans. Inf. Theory **IT-25**, 179 (1979).
[11]H. P. Yuen and V. W. S. Chan, Opt. Lett. **8**, 177 (1983).
[12]G. L. Abbas, V. W. S. Chan, and T. K. Yee, Opt. Lett. **8**, 419 (1983).
[13]L. Mandel, Phys. Rev. Lett. **49**, 136 (1982).
[14]B. L. Schumaker, Opt. Lett. **9**, 189 (1984).
[15]B. Yurke, following paper, Phys. Rev. A **32**, 311 (1985).
[16]A. Yariv and D. M. Pepper, Opt. Lett. **1**, 16 (1977).
[17]M. D. Reid and D. F. Walls, Phys. Rev. A **31**, 1622 (1985).